Multilevel vibrational coherence transfer and wavepacket dynamics probed with multidimensional IR spectroscopy

Matthew J. Nee, Carlos R. Baiz, Jessica M. Anna, Robert McCanne, and Kevin J. Kubarych[a)]
Department of Chemistry, University of Michigan, 930 N. University Ave., Ann Arbor, Michigan 48109, USA

(Received 4 April 2008; accepted 21 July 2008; published online 25 August 2008)

Multidimensional infrared (MDIR) spectroscopy of a strongly coupled multilevel vibrational system $Mn_2(CO)_{10}$ (dimanganese decacarbonyl) in cyclohexane solution reveals fully resolved excited vibrational state coherences that exhibit slow 0.25–0.50 ps^{-1} decay constants. Detailed analysis of the waiting-time dependence of certain cross-peak amplitudes shows modulation at multiple frequencies, providing a direct signature of excited vibrational coherences resulting from coherence transfer. A new signature of coherence transfer is observed as temporally modulated cross-peak amplitudes with more than one modulation frequency. The relative importance of different coherence transfer paths is considered in the context of the orientational response of a system which includes two vibrational modes with parallel dipole moments. Since MDIR spectroscopy enables spectral isolation of individual excited vibrational coherences (i.e., coherences between fundamental excitations), these experiments report directly on the frequency-frequency correlation functions of the excited states relative to each other as well as relative to the ground state. These results highlight the rich information contained in fully exploring three-dimensional third-order spectroscopy, particularly regarding chemically relevant slower dynamics and the importance of intramolecular interactions leading to dephasing by optically dark or low-frequency modes of the molecule.
 [DOI: 10.1063/1.2969900]

I. INTRODUCTION

Multidimensional optical spectroscopy offers direct access to dynamical processes in the condensed phase by spreading spectral information over two or more frequency axes.[1,2] Multidimensional spectra reveal underlying coupling,[3–6] chemical exchange,[7–10] coherence transfer,[6,11–14] spectral diffusion,[15–18] and system-bath interactions that are obscured in a conventional one-dimensional spectrum. Recent observations of excited state vibrational[11] and electronic[13,14,19] coherence in the condensed phase suggest new experimental probes of molecular dynamics that include additional correlations, providing further insight into the relaxation mechanisms responsible for energy flow and dissipation in equilibrium and reacting systems. Coherence between excited electronic states in the Fenna–Matthews–Olson (FMO) energy transport complex, for example, has led to the conclusion that efficient light harvesting is due in part to the preservation of delicate quantum mechanical phase relationships between excited chromophores.[13,14,19] Analogous multidimensional infrared (MDIR) investigation of a metal dicarbonyl complex showed coherence between vibrational states within the manifold of coupled fundamental transitions, as well as coherence transfer and relaxation-induced spectral correlations.[11] Although the details differ, both systems exhibit essential features of quantum dynamics, including dephasing and population relaxation.

Multidimensional spectra enable the dissection of complex condensed phase line shapes by correlating an excited frequency with a detected frequency. From the perspective of the nonlinear response function formalism, between optical interactions the system evolves in either a population (diagonal density matrix element) or a coherence (off-diagonal density matrix element) and the signal is determined by the sum over all such paths. Information on population relaxation is central to a detailed description of anharmonic couplings, Fermi resonances, and solute-solvent interactions, while the relaxation of coherences underlies spectral line shapes. The third-order response, $R^{(3)}(t_1,t_2,t_3)$, has three time intervals, the second of which (t_2) is denoted the "waiting time." Experiments exploring the waiting-time dependence of the two-dimensional (2D) spectrum enable the extraction of population relaxation, orientational diffusion, spectral diffusion, and chemical exchange. In addition to such "incoherent" processes, coherent oscillations in 2D spectral features may also be observed in waiting-time dependent measurements. Coherences, whether electronic,[13,14,19] vibronic,[20–23] or purely vibrational,[11] have been directly observed as oscillations in transient pump-probe and multidimensional spectroscopy. Oscillations of differential absorption features or of cross-peak amplitudes may arise due to coupling between the fast degrees of freedom and the adiabatically separated slow degrees of freedom. Although most investigations have studied slow vibrational modulation of fast electronic absorption, very recently all-infrared pump-probe and 2D experiments have observed

[a)]Author to whom correspondence should be addressed. Tel.: (734)-764-7528. FAX: (734)-647-4865. Electronic mail: kubarych@umich.edu.

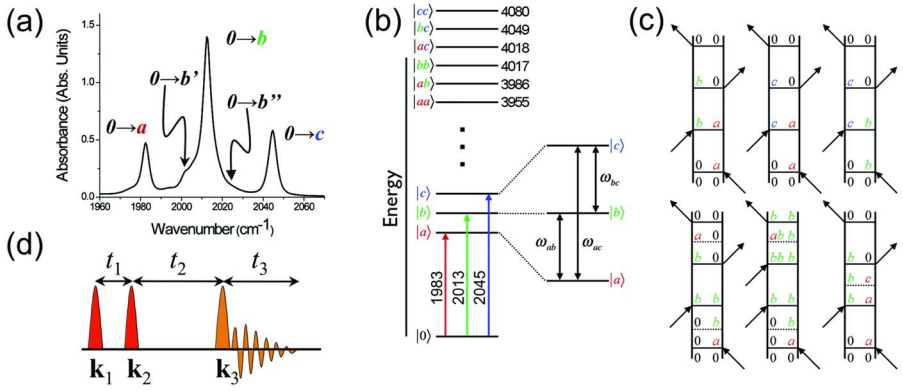

FIG. 1. (Color online) (a) FTIR spectrum of the carbonyl stretching region of DMDC in cyclohexane. Three major peaks are seen, with shoulders on either side of the largest peak (labeled b' and b''). (b) One- and two-quantum vibrational energy levels of the three main bands of DMDC labeled with the IR transition energies relative to the ground state in cm^{-1}, highlighting the states involved in the excited state vibrational coherences. (c) Six representative double-sided Feynman diagrams corresponding to cross peaks which oscillate during the waiting time t_2. The bottom three pathways involve coherence transfer (indicated by the dotted lines) during t_1 and t_3 (left) and during t_2 (right). (d) 2DIR pulse sequence indicating time and wave vector variables.

$\sim$100 cm^{-1} modulations of $\sim$3000 cm^{-1} NH and OH stretch transient absorption in the electronic ground state of hydrogen-bonded dimers through impulsive excitation of low-frequency vibrational modes.[24–29] These experiments are highly sensitive to anharmonic coupling, spectral diffusion, and complex vibrational relaxation pathways.

The coupled vibrations in metal carbonyl complexes are analogous to excitonic multichromophoric systems, where energy level splittings are due not to adiabatic separation of time scales but to the direct coupling of local modes. Resulting from strong interactions with one or more shared metal atom, metal carbonyl complexes exhibit 10–80 cm^{-1} splitting in the CO stretch spectral region[3,6,30] [Fig. 1(a)]. MDIR studies of a rhodium dicarbonyl (dicarbonyl-acetylacetonato-rhodium(I), RDC) have revealed cross peaks between symmetric and antisymmetric coupled CO stretches which have 70 cm^{-1} modulations linked to a coherence between the two excited vibrational levels.[11] Maxima and minima of the vibrational wavepackets were observed in a series of eight two-dimensional IR (2DIR) spectra and the decay of the coherent oscillations was determined by pump-probe transient absorption. Using a model based on a Redfield theory approach, the RDC example clearly showed MDIR spectroscopy to be able to capture the dynamics of population relaxation and coherence transfer.

Using the strongly coupled CO stretching modes of a metal carbonyl $Mn_2(CO)_{10}$ [dimanganese decacarbonyl, DMDC, see Figs. 1(a) and 1(b)], we have applied MDIR spectroscopy to investigate several key features present in recent studies of both electronic and vibrational coherence. By reducing the experimental acquisition time to a few seconds per individual 2DIR spectrum,[31] we resolve multiple low-frequency vibrational coherences as well as signatures of vibrational coherence transfer. The dataset comprised of over 180 2D spectra enables Fourier transformation of each peak in the 2D spectrum as a function of the waiting time, yielding direct determination of the linewidths of the low-frequency modulations attributed to coherences among the excited vibrational states. We find these linewidths to be comparable to those of the fundamental transitions, suggesting that all the excited vibrational states owe their dephasing to the same basic origin. The experimental results are interpreted within the context of the secular approximation to Redfield theory yielding vibrational lifetimes and dephasing rates. The observation of coherence transfer, however, highlights the need for a theoretical treatment including nonsecular terms in the Redfield relaxation tensor. A more detailed analysis presenting a model of the complex multilevel coherence transfer and *ab initio* derived anharmonic force constants is beyond the scope of this paper and will be presented elsewhere.

Coherence transfer in the context used here refers to any transfer of one coherence to another—as shown diagrammatically in the lower half of Fig. 1(c)—and is explicitly neglected in the commonly used secular approximation to Redfield theory.[2,6,11,32–36] The Redfield theory expression for the reduced density operator σ is

$$i\hbar \frac{\partial \sigma(t)}{\partial t} = \mathrm{Tr}_B\{[H(t), \rho(t)]\} \tag{1}$$

where $H(t)$ is the full Hamiltonian of the system H_{sys}, the field-matter interaction H_{int}, as well as system-bath coupling H_{SB}; Tr_B indicates a trace over the bath degrees of freedom; and the full system density matrix is $\rho(t)$. Written in a basis, such as the field-free system eigenstates $(H_{sys}|j\rangle = E_j|j\rangle)$, the equation of motion for the elements of σ are

$$\frac{\partial}{\partial t}\sigma_{jk}(t) = -i\omega_{jk}(t)\sigma_{jk}(t) + \sum_{lm} \Gamma_{jk,lm}\sigma_{lm}(t), \tag{2}$$

where $\Gamma_{jk,lm}$ is the relaxation superoperator and $\omega_{jk} = (E_j - E_k)/\hbar$. The frequency, ω_{jk} is expressed as a time-dependent parameter in anticipation of stochastic models of dephasing. Population relaxation from eigenstate j to k corresponds to the element $\Gamma_{kk,jj}$, decay of a coherence σ_{lm} to a population σ_{kk} is tabulated as $\Gamma_{kk,jm}$, while coherence transfer from σ_{lm} to σ_{jk} is expressed as $\Gamma_{jk,jm}$. This description of relaxation is not general as it explicitly requires a separation of time scales between the system degrees of freedom and those of the bath—an assumption that may not be valid for fundamental chemical processes including solvation and reaction dynamics. Regardless of the limitations of such models, ex-

perimental measurements of population relaxation and phase decoherence are essential for any quantitative comparison to more sophisticated theoretical approaches to quantum dynamics. For the case of DMDC in cyclohexane solution, population relaxation (i.e., the vibrational lifetime) is on the order of 80 ps, while the fundamental transition dephasing rates are ~6 ps (based on a homogeneous linewidth, $\Delta\nu = 5\ \mathrm{cm}^{-1}$); thus the system's dynamics are indeed slower than typical liquid dynamics time scales.[37] Therefore, in the regime where the Markov limit applies and the bath remains at equilibrium, experimental nonlinear spectroscopy reports the elements of Γ. The key feature of this work is the experimental waiting-time dependence of DMDC in cyclohexane recorded over 18 ps in 100 fs steps revealing signatures of vibrational wavepacket motion as well as coherence transfer. Our data present a formidable challenge to theory in order to extract the full dynamical information at the molecular level.

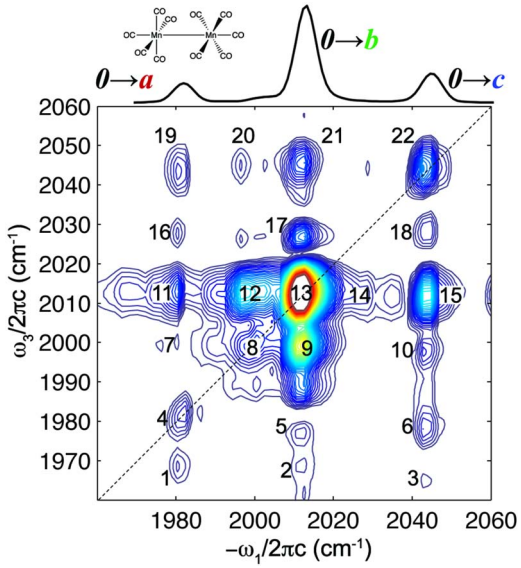

FIG. 2. (Color online) An absolute value rephasing ($\mathbf{k}_s=-\mathbf{k}_1+\mathbf{k}_2+\mathbf{k}_3$) 2DIR spectrum of DMDC in cyclohexane at $t_2=0$ ps shows a large number of peaks, referenced throughout this article as indicated, and detailed in Table I. The FTIR (shown above the 2D spectrum) shows peaks in the same locations. The 2DIR is plotted with 60 evenly spaced contours ranging from 6% to 70% of the maximum intensity.

II. EXPERIMENTAL METHODS

The experimental details of our 2DIR spectrometer have been discussed in detail previously.[31] Briefly, 1 mJ, 100 fs pulses of 800 nm light from a regeneratively amplified Ti:sapphire system (Spectra-Physics Spitfire Pro) are used to pump two independently tunable optical parametric amplifiers (OPAs). The signal and idler from each OPA are difference-frequency mixed in separate 1 mm GaSe crystals to generate midinfrared pulses centered near 5 μm (2000 cm^{-1}). Three such pulses (~500 nJ each) are focused and crossed in the sample at a small angle in a box geometry, allowing the sample to radiate the third-order nonlinear signal in a background-free direction. All three pulses have the same laboratory-frame polarization; the detected signal also has the same polarization. The pulse sequence shown in Fig. 1(d) labels the three pulses ($\mathbf{k}_1$, $\mathbf{k}_2$, and $\mathbf{k}_3$) and their relative timings (t_1, t_2, and t_3) as they are referenced throughout this work. All spectra shown are absolute value rephasing spectra, such that $\mathbf{k}_s=-\mathbf{k}_1+\mathbf{k}_2+\mathbf{k}_3$. A 5 mM solution of DMDC in cyclohexane was used in a sample cell with a thickness of 100 μm created by a Teflon spacer between two 3 mm CaF_2 windows. The signal is collinearly overlapped with a slightly delayed reference local oscillator (identical to the third pump beam, but with about one-tenth the energy) for heterodyne detection. Both the signal and the local oscillator are then upconverted into the visible region of the spectrum by sum frequency generation with a 350 ps [full width at half maximum (FWHM)] chirped pulse centered at 800 nm obtained from the Fresnel reflection from a near normal incidence 1 mm fused silica window (with an antireflection coated rear face) before entrance into the compressor. In our previous report of chirped-pulse upconversion 2DIR spectroscopy,[31] the time delay between the third pump pulse (and therefore the signal) and the chirped pulse was not balanced, meaning that the upconverted light would appear at different visible wavelengths as the t_2 delay is varied due to temporal overlap with different instantaneous frequencies of the chirped pulse. This frequency shift is easily removed by correcting for the spectral phase of the chirped pulse determined independently by frequency-resolved second-harmonic generation cross correlation with a transform-limited 800 nm pulse. In the present work, we have mounted a gold-coated hollow corner-cube retroreflector on the same translation stage that produces the t_2 delay, thus maintaining a constant time delay between the chirped pulse and the generated signal, thus eliminating the need to correct the detected frequency axis.

The collinear upconverted signal and local oscillator fields are dispersed and their spectral interference is recorded on a 1340×100 pixel thermoelectrically cooled charge coupled device array (PI Acton, PIXIS). Collection of a 2DIR spectrum involves recording this heterodyned signal for several thousand different time delays t_1 scanned continuously over a range of 16 ps yielding 2 cm^{-1} resolution. Each frequency element of the signal is Fourier transformed with respect to t_1 to yield a frequency-frequency correlation plot. The data presented here involved collecting such 2DIR spectra for waiting time (t_2) delays ranging from −1 to 18 ps in 0.1 ps steps. This range requires on the order of 1 h to collect, making it straightforward to ensure that the signal level does not degrade during the course of the measurement.

III. RESULTS

A. Two-dimensional spectra at $t_2=0$

An absolute value rephasing 2DIR spectrum ($t_2=0$ ps) of DMDC in cyclohexane is shown in Fig. 2. The t_1 axis has been zero padded with an additional 10 000 time points (in addition to the approximately 5000 points collected) prior to Fourier transforming along that axis into the frequency domain. A full list of the peak positions can be found in Table I, in which each peak is assigned a numerical label for reference. As expected, the diagonal peaks are very similar to the Fourier transform infrared (FTIR) spectrum shown in

TABLE I. Peaks present in the 2DIR spectrum of DMDC in cyclohexane. Transition dipoles listed reference the energy level diagram in Fig. 1(b); Liouville paths involving coherence transfer effects are neglected in the assignments.

Peak label	Peak coordinates (cm^{-1}) $(-\omega_1, \omega_3)$	Transition dipoles involved	
		ω_1	ω_3
1	(1983, 1972)	0-*a*	2*a*-*a*
2	(2015, 1972)	0-*b*	*ab*-*b*
3	(2044, 1972)	0-*c*	*ac*-*c*
4	(1983, 1983)	0-*a*	*a*-0
5	(2015, 1983)	0-*b*	*a*-0
6	(2044, 1983)	0-*c*	*a*-0
7	(1983, 2002)	0-*a*	*b*′-0 or *ba*-*a*
8	(2002, 2002)	0-*b*′	*b*′-0
9	(2015, 2002)	0-*b*	*b*′-0 or 2*b*-*b*
10	(2044, 2002)	0-*c*	*b*′-0 or *bc*-*c*
11	(1983, 2015)	0-*a*	*b*-0
12	(2002, 2015)	0-*b*′	*b*-0
13	(2015, 2015)	0-*b*	*b*-0
14	(2025, 2015)	0-*b*″	*b*-0
15	(2044, 2015)	0-*c*	*b*-0
16	(1983, 2028)	0-*a*	*ac*-*a*
17	(2015, 2027)	0-*b*	*bc*-*b*
18	(2044, 2029)	0-*c*	2*c*-*c*
19	(1983, 2044)	0-*a*	*c*-0
20	(2002, 2044)	0-*b*′	*c*-0
21	(2015, 2044)	0-*b*	*c*-0
22	(2044, 2044)	0-*c*	*c*-0

Fig. 1(a) and reproduced at the top of Fig. 2. Table I also includes the available assignments to the various transitions involved in the peaks seen in Fig. 2. There are three dominant peaks along the diagonal, plus a small shoulder peak (**8**) just to the red of the largest center peak. These four peaks are associated with the ground state to first excited state transitions for the states ***a***, ***b′***, ***b***, and ***c*** shown in the FTIR spectrum in Fig. 1. Cross peaks arising from each possible combination of ω_1 and ω_3 values are seen. All nine major peaks (the peaks corresponding to the diagonal and cross peaks) have smaller peaks beneath them which have the same value for ω_1, but a slightly lower value of ω_3. These peaks represent the Liouville paths involving transitions between the first (fundamental) and second (overtone) sets of excited state energy levels [see Fig. 1(b)]. These cross peaks report on the anharmonicity of the vibrational potential:[3,38] the diagonal anharmonicity (the difference in energy between the $0\rightarrow1$ and $1\rightarrow2$ transition energies of a given mode) of a single mode may not be the same as the off-diagonal anharmonicity, which reports on the coupling between modes.[30] The line shape of each of the major peaks is similar, and profiles showing similar spectral widths are seen along the diagonal and antidiagonal axes of each peak.

B. 2DIR spectra as a function of waiting time t_2

Several 2DIR spectra taken at increasing values of t_2 are shown in Fig. 3. As the waiting time increases, the diagonal peaks decay in amplitude, while the other peaks decay and oscillate. By integrating nine experimental pixels (spanning about 5 cm^{-1} along ω_1 and 3 cm^{-1} along ω_3) in the 2D spectrum for each peak as a function of time, we are able to monitor quantitatively the evolution of the salient features of the spectrum. These are grouped according to their behavior as a function of the waiting time, t_2. Some peaks show only decay over the course of the measurement. This group includes the diagonal peaks and the singly excited to doubly excited transition peaks (the "overtone" peaks) for ***a*** and ***b***. These are plotted in Fig. 4. The decay can be fitted to a biexponential for each of the peaks, providing insight into the intramolecular vibrational redistribution, vibrational lifetime, and orientational dephasing rates (tabulated in the supplemental information).[39] Based on the antidiagonal peak widths, the dephasing times for all diagonal peaks range from 5 to 6 ps, while similar lifetimes are observed for the anharmonic peaks beneath them.

Some peaks show clear oscillation as a function of t_2; examples are shown in Fig. 5. Peaks **5**, **6**, **11**, **15**, **19**, and **21** all belong to this group. These six can be further subdivided into three pairs of peaks, where each pair oscillates at the same frequency and with the same phase. Fourier transforms (shown in the right column of Fig. 5) of the oscillations show that two of these pairs, (**5**, **11** and **15**, **21**) have the same center frequency oscillations (centered near 30 cm^{-1}), while the third pair oscillates at 64 cm^{-1}, and has a slightly narrower frequency spectrum. The center frequencies and widths as determined by Lorentzian fits are listed in the supplemental data Table S-II.[39]

Some peaks show more than one oscillation as a function of t_2. The trace for peak **3** is shown in Fig. 6(a). The FT [Fig. 6(b)] in this case shows both frequencies (30 and

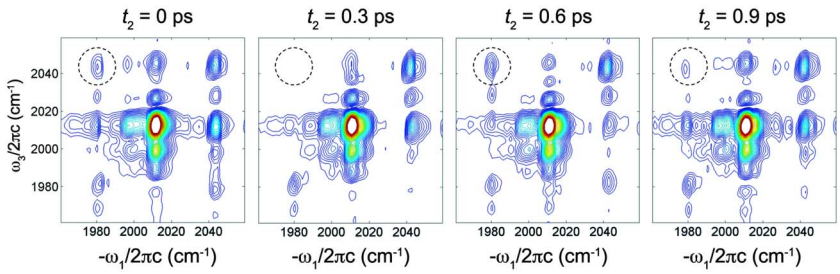

FIG. 3. (Color online) A series of four 2DIR spectra of DMDC in cyclohexane, taken at different waiting times t_2. Integrating the volume of the circled peak as a function of time delay shows oscillatory behavior caused by the waiting-time excited-state coherence. Oscillation arises because of the two Liouville paths contributing to that 2DIR peak; one involves a ground-state population during t_2 while the other contains a coherence between states *a* and *c*. The circled peak is peak 19, which oscillates at 64 cm^{-1} (1.1 ps period).

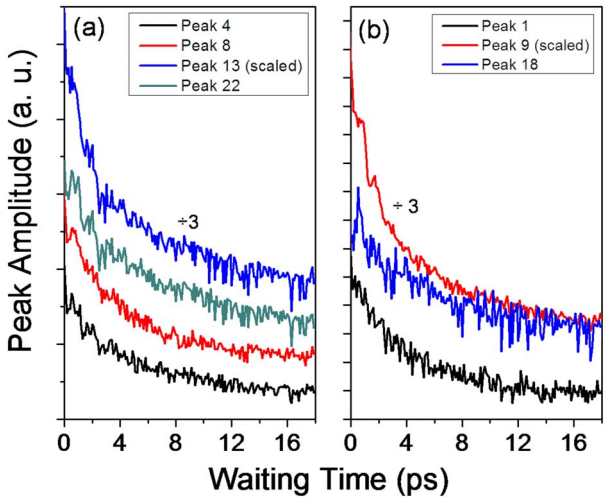

FIG. 4. (Color online) Peak volumes of the diagonal peaks (a) and the peaks directly beneath them (b) as a function of waiting time. The peaks with the lower value of ω_3 correspond to paths which go through an overtone in the mode whose diagonal peak has the same value of ω_1. The largest peaks in each panel (peaks 13 and 9) have been scaled by a factor of 3 to show the relative intensities on the same plot. As tabulated in the supplemental information, biexponential fits to the decays show fast decay times ranging between 2.5 and 4 ps for all peaks shown here (Ref. 39).

60 cm^{-1}) observed in the fundamental peaks. The FT peaks are similar in width to those seen in the corresponding fundamental peaks. Peak **10** [Figs. 6(c) and 6(d)] shows a single oscillation frequency of 30 cm^{-1}; the frequency width is appreciably broader than in the other oscillatory peaks, consistent with the seemingly faster oscillation decay in the time domain. Peak **2** [Figs. 6(e) and 6(f)], the off-diagonal peak with the most rapidly decaying oscillation, shows effectively no peak in the FT, presumably because the oscillation is damped so heavily that the FT signal is too broad to be separated from the noise. For each of the peaks **3**, **10**, and **2**, analogous peaks **16**, **17**, and **7**, respectively, show similar time-dependent behavior. A full set of t_2-dependent 2DIR spectra is available as a supplemental movie file.[39]

IV. DISCUSSION

A. General vibrational structure

The 2DIR spectrum at $t_2=0$ provides new information about the vibrational structure of DMDC. It is important to note that, although there are a large number of peaks in the 2DIR spectrum, those corresponding to fundamental (singly excited) transitions can be associated with features in the linear FTIR spectrum. The largest peak in the spectrum (peak **13**) has shoulders on either side in the FTIR as well as the diagonal of the 2DIR spectra. Consequently, each of these peaks can have cross peaks with each of the other major peaks visible in the FTIR. The three largest peaks are assigned to three normal modes calculated previously[40] (referred to here as levels ***a***, ***b***, and ***c***). Previous normal mode analysis[40] confirmed the presence of four IR active CO stretching modes, whose transition dipole moments and directions were calculated. The calculation showed that the transition dipole moments between the ground state and the lowest and highest CO frequency modes are, in fact, parallel to each other (each belongs to the irreducible representation B_2 under the D_{4d} point group), but perpendicular to those corresponding to the two (degenerate E_1) modes responsible for the more intense absorption feature in the center. These two degenerate modes have transition dipole moments orthogonal to one another as well. The peaks involving these modes are the primary focus of our discussion. Other normal modes which would typically be considered symmetry forbidden may have non-negligible IR transition dipole moments which, though forbidden within the harmonic approximation, are weakly infrared active and may be responsible for the shoulders observed here and in previous studies. A full understanding of the smaller amplitude peaks will require higher level electronic structure calculations, work that is currently underway.

The anharmonicities of the different modes can be determined from the smaller peaks beneath the diagonal peaks and their corresponding cross peaks: those peaks directly under diagonal indicate the difference $\Delta_{xx}=\omega_{x-0}-\omega_{2x-x}$, where

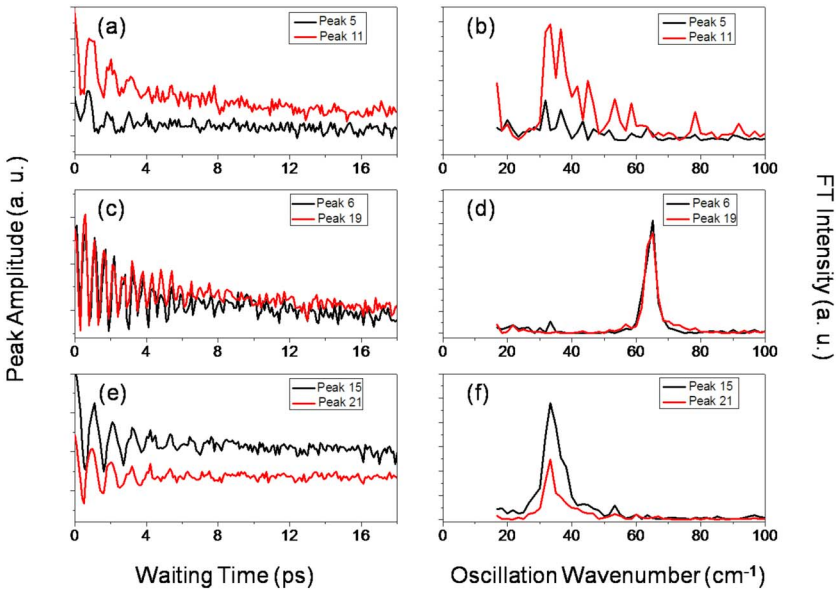

FIG. 5. (Color online) Peak volumes and respective Fourier transform amplitudes of peaks 5 and 11 [(a) and (b)], 6 and 19 [(c) and (d)], and 15 and 21 [(e) and (f)] as a function of waiting time. Each pair oscillates at a frequency as shown in the absolute value of the Fourier transform of the time-domain volumes.

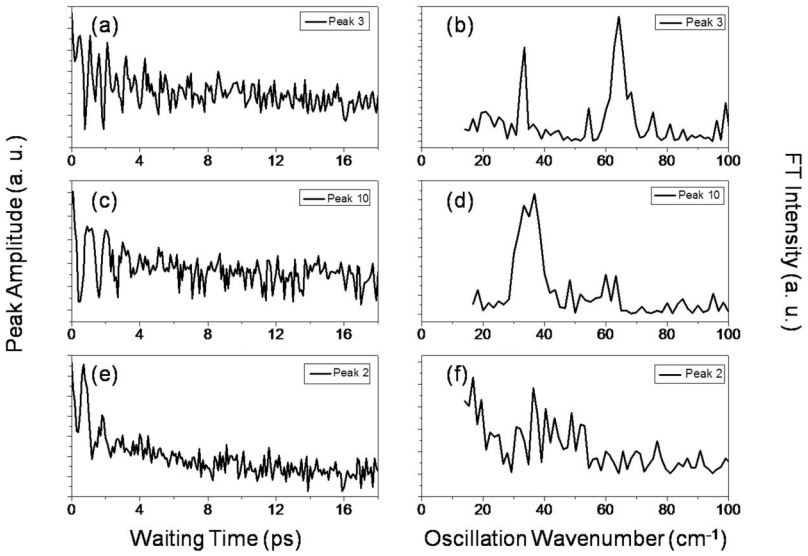

FIG. 6. Peak volumes and their respective Fourier transforms of some of the peaks accessing combination bands. Peak 3 (a) clearly oscillates at the same two frequencies [Fourier transform in (b)] seen in Fig. 4. Peaks 10 [(c) and (d)] and 2 [(d) and (e)], however, show at best only a single broad peak.

ω_{2x-x} is the frequency of the transition from the first overtone of mode $\boldsymbol{x}$ to its fundamental. It is clear by inspection that the diagonal anharmonicities are all approximately the same ($\Delta_{aa}=11$ cm^{-1}, $\Delta_{bb}=13$ cm^{-1}, $\Delta_{cc}=15$ cm^{-1}). These values are consistent with CO stretches observed in other metal carbonyl complexes.[6,30,41] Based on the usual third-order response function for 2DIR, which neglects all terms $\Gamma_{jk,lm}$ from Eq. (2) that model coherence transfer, for example, each fundamental peak should have one peak beneath it, reporting on the difference between the sum of the fundamentals involved and the actual energy difference between the combination band and the observed ω_3 value. Considering peak **2**, for example, $\omega_3=1972$ cm^{-1} is 11 cm^{-1} less than the loss of a quantum of mode $\boldsymbol{a}$ (1983 cm^{-1}) would be under the uncoupled harmonic oscillator picture. These off-diagonal anharmoncities, then, are defined by

$$\Delta_{xy}=(\omega_{a-0}+\omega_{b-0})-(\omega_{ab-b}+\omega_{b-0}), \tag{3}$$

which simplifies to

$$\Delta_{xy}=(\omega_{a-0}-\omega_{ab-b}). \tag{4}$$

In DMDC, it appears that the off-diagonal anharmonicities are nearly identical to the diagonal anharmonicities to within the experimental resolution. The energy level diagram shown in Fig. 1(b) includes the energy levels (in cm^{-1}) for the one and two quantum states as determined by our 2DIR spectra.

A brief comment regarding peak **14** is warranted. The FTIR spectrum shown in Fig. 1(a) shows a very slight shoulder on the higher frequency side of the $\boldsymbol{0}\rightarrow\boldsymbol{b}$ transition peak (labeled $\boldsymbol{b''}$). This peak is brought to greater prominence in cross peaks in the 2DIR spectra, despite the effectively invisible diagonal peak. This is possible because cross-peak amplitudes are weighted by the product of four different transition dipole moment magnitudes. Thus, cross peaks involving one very weak and one very strong transition (such as peak **14**) are likely to have a larger peak volume than the diagonal peak for the weaker dipole transition, particularly if the two dipoles are not perpendicular. This effect is seen at some waiting times for peak **17**. Table I indicates that peaks **16**, **17**, and **18** have values of ω_3 which are very similar to the expected frequency of the $\boldsymbol{0}\rightarrow\boldsymbol{b''}$ transition. Because the peaks arising from transitions involving two quantum states have opposite sign from those which access only one quantum states, the occurrence of both a cross peak with the $\boldsymbol{0}\rightarrow\boldsymbol{b''}$ state and the two quantum transition in the same place will appear in the absolute magnitude spectrum as a single peak with the overall intensity and profile of the difference of the two contributing paths. As such, at some waiting times, peak **17** appears more like two peaks because at this location in the spectrum the path giving rise to the cross peak between $\boldsymbol{0}\rightarrow\boldsymbol{b''}$ and $\boldsymbol{0}\rightarrow\boldsymbol{b}$ is similar in magnitude, but opposite in sign, to the path which accesses the two-quantum state $\boldsymbol{bc}$-$\boldsymbol{c}$.

A few peaks cannot be unambiguously assigned (**7**, **9**, and **10**). Because the energy difference between the levels $\boldsymbol{b}$ and $\boldsymbol{b'}$ is very similar to the observed anharmonicities in the diagonal peaks, we are unable to distinguish the relative contributions of these two paths to the peaks noted. We must approach them as possessing contributions from each. Since the spectra presented here are absolute values of the rephasing part of the spectrum only, our overtone and combination band peaks do not show opposite sign to that of the fundamentals. Although work in our laboratory is underway to improve the efficiency with which absorptive spectra are collected, the time to collect the necessary data for a set of 180 t_2-dependent absorptive spectra is prohibitively long compared to the work presented here. The features seen in the spectra at different values of t_2, however, are well presented by the absolute value of the rephasing spectra.

We can see that the peaks in the cyclohexane solution of DMDC are homogeneously broadened; the antidiagonal and diagonal widths for all the diagonal peaks are both approximately 7 cm^{-1}. The widths of the peaks in the FT with respect to t_2 are approximately the same as those of the antidiagonal widths of the fundamental transitions. As detailed further in the next section, this similarity in the spectral widths suggests that the fluctuations of the excited state energy levels for different modes are uncorrelated. Again, these results are consistent with calculations and experiments on other metal carbonyl systems.[30,41]

In previously studied two excited state systems such as RDC and its iridium counterpart, IDC, the parameters extracted from the 2DIR experiment were modeled as two coupled anharmonic oscillators. This method, which successfully determines a reasonable set of coupling parameters that can be calculated from and compared to *ab initio* electronic structure results, is not employed here despite its earlier successes. Although the delocalized normal modes could be written in the basis of the local oscillators, q_i, the number of CO modes (ten—one corresponding to each CO group) is far too large to allow a unique determination of the modes. Although only three major peaks appear in the spectrum, one is attributed to two degenerate states. Expressing the coupled anharmonic potential as

$$V(q_i, \ldots, q_n) = \sum_{i,j}^{n} \alpha_{ij} q_i q_j + \sum_{i,j,k}^{n} \beta_{ijk} q_i q_j q_k + \cdots, \tag{5}$$

for $n=4$, and truncating at terms quartic in the coordinates q_i (cubic anharmonicity) leads to a potential with 31 different fitting parameters, far too many to provide a reliable fit which is unique enough for valid comparison to *ab initio* calculations of molecular structural parameters. Further, several modes in the same spectral region (two at 1953 cm^{-1}, one at 1981 cm^{-1}, two at 2009 cm^{-1}, and one at 2111 cm^{-1}, all determined based on combination bands and overtones)[40] are dark to the IR but are still likely to contribute significantly through intramolecular vibrational relaxation. Although fifth-order 2DIR experiments aid in removing some of the ambiguity of fitting a spectrum with so many peaks, in this case, we are able to assign our third-order spectrum adequately for the purposes of identifying the peaks. Finer improvements to the anharmonicity values are not likely to improve our understanding of the waiting-time dependence of the peaks in the 2DIR spectrum, which is the primary objective of this work.

B. Evolution of 2DIR spectra with increasing waiting time

The waiting-time dependence of each peak in the 2DIR spectrum can be assigned to one of several groups. The first group includes the diagonal peaks and their overtones. These are the peaks shown in Fig. 4. A biexponential decay describes the behavior of these peaks: for each, the faster decay corresponds to intramolecular vibrational relaxation, while the overall vibrational lifetime accounts for the slower decay. Reasonable quality 2DIR spectra could be obtained for waiting times longer than 80 ps, implying that the system-bath coupling responsible for vibrational population relaxation is relatively weak. The overtone peaks are as distinguishable at 80 ps (aside from the general loss of signal-to-noise ratio with increasing time) as they are at 0 ps, which we take as evidence against the long-time signal arising from a thermal grating in our sample created by our first two IR pulses. Each of the next set of peaks (peaks **5**, **6**, **11**, **15**, **19**, and **21**, Fig. 5) shows one frequency of oscillation in the waiting-time dependence. This is identical to behavior noted for cross peaks in RDC: the oscillation arises because the system exists in a coherence (denoted by $\boldsymbol{x}$-$\boldsymbol{y}$, to distinguish coherences from field-induced transitions, $\boldsymbol{x} \rightarrow \boldsymbol{y}$, in which excitation or de-excitation occurs) of two excited vibrational levels during the waiting time t_2.[11] Creating a coherence implies that the third field-matter interaction involves a transition probability which oscillates in time, leading to oscillations in the corresponding peaks in the 2D spectrum. This effect is seen more clearly in the Feynman diagrams shown in the upper row of Fig. 1(c): excited state coherences appear during t_2 for all three of these diagrams, in addition to the ground-excited state coherences always shown during t_1 and t_3. The frequency of the peak amplitude oscillation is determined by the difference frequency between the two energy levels involved in the coherence. Since only the singly excited states ($\boldsymbol{a}$, $\boldsymbol{b}$, and $\boldsymbol{c}$) can be accessed by $\mathbf{k}_1$ and $\mathbf{k}_2$, there are only three possible combinations of two states to be involved in a waiting-time coherence for DMDC. Further, because two of these combinations have the same difference frequency ($\omega_{a\text{-}b}=\omega_{b\text{-}c}=30$ cm^{-1}) only two different possible oscillation frequencies are expected. The FT oscillations shown in Fig. 5 are in excellent agreement with this expectation: each pair shown has a Liouville path which passes through a coherence during the waiting time, corresponding to the state excited by $\mathbf{k}_1$ and the state emitting to the ground state during t_3 [Fig. 1(c)]. That peaks **16**, **17**, and **18** oscillate only at either 30 or 64 cm^{-1} as expected above also strengthens our assignment of these peaks primarily to paths arising from combination bands rather than as cross peaks with state $\boldsymbol{b}''$. Were there significant contributions from $\boldsymbol{b}''$, each of these peaks would oscillate at an additional frequency corresponding to the difference between the excitation frequency and 2025 cm^{-1} (the frequency of the $\boldsymbol{0} \rightarrow \boldsymbol{b}''$ transition). Thus, the FT of peak **16** would, for example, show a peak at 42 cm^{-1} which would be readily distinguished from 30 or 64 cm^{-1}.

A 2D spectrum enables the determination of the homogeneous linewidth of a transition by measuring the antidiagonal width about a given center frequency.[42–45] The pure dephasing is therefore distinguishable from the dephasing due either to static frequency distributions or to slowly evolving spectral diffusion (i.e., inhomogeneous broadening). Cross-peak line shapes also indicate correlations between excited and detected frequencies within an inhomogeneously broadened band.[46] In the presence of inhomogeneous broadening, for example, a positive frequency correlation has been observed through cross-peak asymmetry in RDC in chloroform, whereas no asymmetry was observed in cyclohexane solution. In the absence of inhomogeneous broadening, however, there is information that is not straightforwardly obtained from a single 2D correlation spectrum, namely, the frequency-frequency *cross correlation* (FFCC) between two different transitions. The homogeneous linewidths of individual transitions are given by the antidiagonal widths, which are related to the frequency-frequency autocorrelation functions.[47] Without inhomogeneous broadening, no form of correlation (positive, negative, or zero) of frequency fluctuations of the coupled transitions is expected to lead to skewed diagonal or cross-peak line shapes. Regardless, direct determination of the relative frequency-frequency cross correlations is, in principle, possible by examining the dephasing of coherences *among* the excited vibrational states

(i.e., σ_{ab}, σ_{bc}, or σ_{ac}) and comparing these linewidths to those observed for the fundamental transitions (i.e., σ_{0a}, σ_{0b}, or σ_{0c}). Instantaneous frequency trajectories of two fundamental transitions (***a*** and ***b***), one from the state ***0*** to the state a, and the other from ***0*** to ***b***, can be written in terms of the average transition frequencies $\langle\omega_{0-a}\rangle$ and $\langle\omega_{0-b}\rangle$, and their fluctuations $\delta\omega_{0-a}(t)$ and $\delta\omega_{0-b}(t)$:

$$\omega_{0-a}(t) = \langle\omega_{0-a}\rangle + \delta\omega_{0-a}(t),$$
$$\omega_{0-b}(t) = \langle\omega_{0-b}\rangle + \delta\omega_{0-b}(t). \tag{6}$$

A coherence between these two excited states evolves at the difference of these two excited energy levels with a frequency trajectory given by

$$\omega_{0-a}(t) - \omega_{0-b}(t) = \langle\omega_{0-a}\rangle - \langle\omega_{0-b}\rangle + [\delta\omega_{0-a}(t) - \delta\omega_{0-b}(t)]. \tag{7}$$

If the fluctuations are truly identical, the difference frequency becomes a constant regardless of the nature of the time scale of the correlation function of the fluctuations, whether slow (inhomogeneous limit) or fast (homogeneous limit). Moreover, recent theoretical and experimental results for water dissolved in acetonitrile suggest that different vibrational modes on the same molecule can have qualitatively different dephasing dynamics.[48] Observation of long-lived electronic coherence in the FMO complex led to the conclusion that the protein environment, which may be viewed to act as a bath, induces correlated fluctuations among the excited exciton bands, preserving the coherence well beyond the known electronic dephasing time.[13,14,19] In another example, for a simulated dipeptide system where the two coupled amide I transitions were modeled with independent baths the dephasing of excited state coherence was found to occur on roughly the same time scale as the dephasing of fundamental transitions.[49]

The data presented here show signatures of both coherence transfer and vibrational wavepacket motion in a complex anharmonically coupled metal carbonyl system. A signature of vibrational coherence transfer is observed as modulations of certain cross peaks that show multiple frequency components in the Fourier spectrum of the modulations. The qualitative interpretation of the results presented here will aid in constructing a systematic approach to interpreting spectra of complex multilevel systems with temporally overlapping population relaxation and coherence transfer beyond the secular approximation of Redfield theory.

The widths of the Fourier transform peaks (FWHM of a fit of the FT amplitude to a Lorentzian line shape) indicate that the coherences decay in a matter of a few picoseconds, slightly faster than the fundamental vibrational dephasing time obtained by inverting the antidiagonal spectral widths, but still long lived enough to have undergone several periods. This similarity of time scales suggests that frequency fluctuations of the energy levels of the two states involved in the coherence relative to one another appear to result from effectively independent baths. If the baths were correlated, the frequency fluctuations would reflect such correlations, resulting in slower dephasing. Information about the relative frequency fluctuations of excited states based on multidimensional experiments has been reported previously in a bacterial reaction center and in the FMO complex.[13,14,19] However, little is known about the precise effects of the solvent environment, and whether intramolecular bath modes (dark states, low-frequency modes, etc.) may play a demonstrable role in the relative correlation of the frequency fluctuations in highly coupled molecules such as DMDC. If the rate of decay of the t_2-dependent coherent oscillations changes with solvation environment, it would indicate that each vibrational mode is coupled to the bath in a different way.[48] In such a case, the relative frequency fluctuations of pairs of modes will evolve in a differently correlated way than in a relatively weakly interacting solvent such as cyclohexane. Both solvent polarizability and dipole moment could figure prominently into the extent and nature of the FFCC in highly coupled vibrational systems; further experiments are already underway in our laboratory to investigate these effects. Presently, however, we explore the effect of cyclohexane, a low-dipole moment, low polarizability solvent. Owing to their surprising complexity, the peaks accessing overtone and combination band states will be discussed in considerable detail within the context of coherence transfer.

C. Coherence transfer pathways

Theoretical treatments of condensed phase spectroscopy often employ the secular approximation to the full equation of motion for the reduced density matrix [Eq. (2)]. The secular terms of the Redfield tensor [cf. Eq. (2)]—Γ_{jjkk} and Γ_{jkjk}—give rise to exponential relaxation of populations (σ_{jj}) and coherences (σ_{jk}), but do not permit evolution of a coherence to a population, or from one coherence to another coherence. The latter process has been observed in vibrational and electronic systems prior to the present work, and such coherence transfer pathways offer additional information regarding the microscopic nature of the system-bath interactions, though its full extraction presents a significant analytical challenge. Such nonsecular terms become non-negligible when the energy differences between eigenstates are small and when relaxation involves many states including both optically bright and dark states.

Unlike the fundamental-only peaks, those peaks accessing combination bands prior to emission show one of two patterns as a function of t_2: either they present two oscillation frequencies (ω_2), or they exhibit one peak which is broader in frequency than its single-excitation counterpart. Both peaks involving a waiting-time coherence (see Fig. 6) between states ***a*** and ***c*** in DMDC clearly show *two* narrow peaks, indicating that an additional coherence contributes to that peak. One possible explanation is that ground-excited state coherence transfer occurs during both t_1 and t_3. Evidence for such coherence transfer, discussed in the introduction and depicted diagrammatically in Fig. 7, has been seen in other metal carbonyl compounds.[11] Although this explanation is one possibility, it is not immediately clear why the effect would be so apparent in some peaks, like peaks **3** and **16**, and effectively invisible for other peaks resulting from similar paths. Further, it is not immediately clear why the

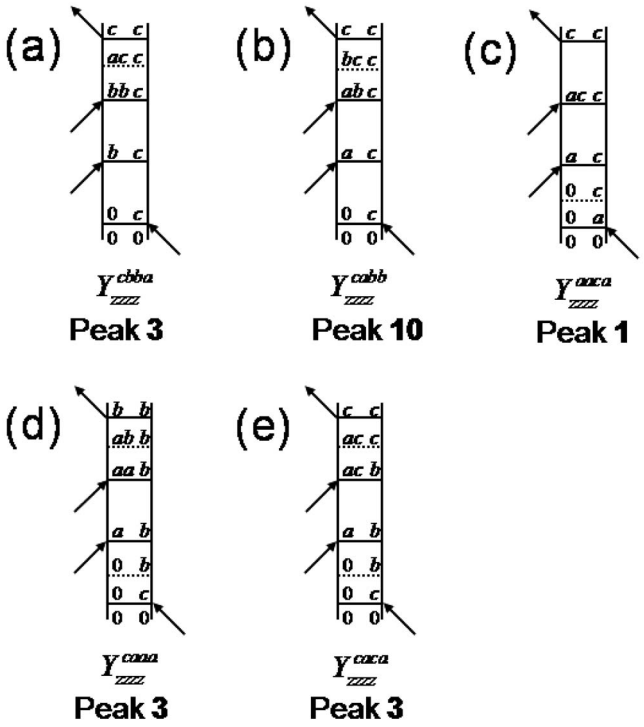

FIG. 7. Representative double-sided Feynman diagrams involving single (1CT) and double (2CT) coherence transfers. 1CT paths can lead to additional oscillations beyond what would be expected by neglecting coherence transfer. Paths leading to these ω_2 oscillations give rise to peaks 3 (a), 10 (b), and 1 (c). While less likely than 1CT paths, 2CT paths contribute significantly to peak 3, as in (d) and (e), but much less to the other peaks.

effect is seen in the peaks involving the second excited states, but not in those which access only the ground and first excited states. If coherence transfer from ***0-a*** to ***0-b*** is prominent, it should lead to additional oscillations in the diagonal and fundamental-only cross peaks. That we do not observe such oscillations may be due to the small contribution relative to other paths, such as those leading to diagonal peaks without coherence transfer. By contrast, such coherence transfer may also explain the broader frequency distribution of the oscillations seen in peaks **2**, **7**, and **10**. In all of these cases, the possible coherences necessarily involve level b, meaning that both oscillation frequencies are nearly 30 cm^{-1}. Although the two difference frequencies are very similar to within the widths of the peaks in our 2DIR spectrum, they may be different enough to account for the broad frequency distribution of these peaks.

It is surprising to find that two peaks (**3** and **16**), both of which involve accessing the combination bands between states ***a*** and ***c***, oscillate at more than one frequency as a function of the waiting time t_2. This suggests that multiple paths involving at least two different coherences during t_2 contribute appreciably to each of these paths. In the absence of coherence transfer, the only possible coherence which could be encountered during the Liouville paths leading to, for example, peak **3** involves the two states ***a*** and ***c***, thereby accounting for the oscillation at 60 cm^{-1} as explained above. To explain the presence of the 30 cm^{-1} oscillation (which could arise from the coherences ***a-b***, ***b-c***, or their conjugates), we turn again to coherence transfer, this time in greater detail.

It has been observed in previous studies of vibrational coherence transfer in third-order nonlinear IR experiments that, assuming that the vibrational transition dipole moment orientations are orthogonal, no Liouville paths including exactly one coherence transfer (CT) event contribute to the final trace over the reduced density matrix, σ.[6] This is not because valid paths cannot be written, but because their orientational response functions necessarily vanish by symmetry. The full response function for a given Liouville path can be expressed as a separable product of two responses. The first, $R_n^{\nu\kappa\chi\lambda}$, describes the vibronic response (i.e., the four ordered field-matter interactions $\mu_\nu,\mu_\kappa,\mu_\chi,\mu_\lambda$) in the absence of the effects of orientational diffusion. Thus far, our discussion has been limited to $R_n^{\nu\kappa\chi\lambda}$. The second term, $Y_{ijkl}^{\nu\kappa\chi\lambda}$, describes the orientational response. Together, the overall response R is the sum over all paths and is given by

$$(R_n)_{ijkl}(\tau_3,\tau_2,\tau_1)=\sum_{\nu,\kappa,\chi,\lambda} R_n^{\nu\kappa\chi\lambda}(\tau_3,\tau_2,\tau_1)Y_{ijkl}^{\nu\kappa\chi\lambda}(\tau_3,\tau_2,\tau_1). \tag{8}$$

In this notation, i,j,k,l are the laboratory-frame polarization directions of the fields involved in the four field-matter interactions (all of which are parallel in our case, so that $i=j=k=l\equiv z$), while the Greek indices ν,κ,χ,λ are the molecule-frame orientations of the dipole moments involved in each interaction. Each orientational tensor $Y_{ijkl}^{\nu\kappa\chi\lambda}$ has been calculated previously for dipole interactions with arbitrary relative angles.[30,50] For a system with two perpendicular vibrational modes (the relative angle between transition dipole moments, $\theta=90°$), paths which arise from one interaction with one dipole and three interactions with the other dipole such as Y_{zzzz}^{aaba} vanish by symmetry. This symmetry exists for both RDC and IDC, but does not hold for the three principal vibrational modes in DMDC. As noted above, $\hat{\mu}_{0\text{-}a}\|\hat{\mu}_{0\text{-}c}\perp\hat{\mu}_{0\text{-}b}$ (regardless of which of the two degenerate ***b*** modes is involved), so a reconsideration of the orientational response is necessary. The tensor Y_{zzzz}^{aaba} continues to vanish by symmetry, but a similar path in which $\mathbf{k}_3$ interacts with $\hat{\mu}_c$ instead of $\hat{\mu}_b$ is associated with the now *nonvanishing* tensor Y_{zzzz}^{aaca}. Thus, several paths that would vanish in a system with three orthogonal modes are now allowed. Such paths appear when coherence transfer is permitted during the various time delays between field-matter interactions. For example, previous third-order experiments have not needed to consider paths involving only a single coherence transfer event (1CT). Nearly all paths generated by 1CT in an orthogonal two-mode system have vanishing orientational contributions to the total response so that all such paths are justifiably neglected in the 2D spectrum. Thus, discussions of vibrational coherence transfer in RDC have focused on paths involving double coherence transfer (2CT). For DMDC, 216 paths involving single coherence transfer can be written (72 each from the initial excitation of one of three modes), 25 of which have nonzero orientational responses owing to the parallel nature of the dipole moments in modes ***a*** and ***c***. For the purposes of this discussion, we have neglected those paths that include "trivial" coherence transfers in which the

relevant density matrix element switches from one coherence to its conjugate (e.g., $|a\rangle\langle b| \rightarrow |b\rangle\langle a|$). The nonvanishing Liouville paths, including 1CT and 2CT paths, for two representative peaks (**3** and **10**) are given in the supplemental information.[39] Interestingly, only 12 possible 1CT paths exist in which the coherence transfer event occurs during t_2, none of which contributes to the total signal because of vanishing orientational response functions. 1CT paths in which the transfer occurs during t_1 or t_3, however, contribute to the overall signal, and may change the oscillations observed during t_2. It should be stressed that, although we observe this evidence for coherence transfer by monitoring our 2DIR spectrum as a function of t_2, we are unable to distinguish paths undergoing 1CT during the different time delays from one another.

We are now in a position to consider the implications of including various 1CT and 2CT paths on the oscillations seen in our spectra as a function of t_2. For the purposes of discussion, we will consider only the 1CT and 2CT paths for a limited number of peaks in the 2D spectrum, specifically peaks **1**, **3**, and **10**. In particular, we wish to determine the origin of the two ω_2 peaks in the FT of peak **3** in a manner consistent with the single, though somewhat broad oscillation frequency in peak **10** and the small amplitude oscillation of peak **1**. Double-sided Feynman diagrams corresponding to some representative 1CT and 2CT Liouville paths (those leading to peaks **1**, **3**, and **10**) are shown in Fig. 7. As has been done previously,[51] we assume that the dipole orientations for successive excitation within a given vibrational mode are parallel. For example, $\hat{\mu}_{a\text{-}0} \| \hat{\mu}_{aa\text{-}a} \| \hat{\mu}_{ab\text{-}b}$. As mentioned in Sec. IV A, the diagonal and off-diagonal anharmonicities for all three modes and their combinations are very similar. Thus, we are unable to separate experimentally contributions from, for example, a path with final field interaction $\boldsymbol{ac} \rightarrow \boldsymbol{c}$ and one which ends with $\boldsymbol{ab} \rightarrow \boldsymbol{b}$; more than one transition has the same frequency ω_3. Because each of these paths would lead to different oscillation frequencies (as in peak **3**, which could arise from each of the two paths just identified), the peak in the 2DIR spectrum appears to oscillate at more than one frequency. It is important to note that the multiple oscillation frequencies do not appear only because the anharmonicities are similar. Some paths, such as the one shown in Fig. 7(e), have the same initial excitation ($\boldsymbol{0} \rightarrow \boldsymbol{a}$) and final emission ($\boldsymbol{ac} \rightarrow \boldsymbol{a}$) as the 0CT paths, but have an oscillation at 30 cm^{-1} during t_2 owing to the waiting-time coherence between states $\boldsymbol{a}$ and $\boldsymbol{b}$. In either case, multiple peaks in the ω_2 spectra are only explained as a result of coherence transfer processes.

Considering only the 1CT paths, we already see that one of the five nonvanishing paths which leads to peak **3** goes through the coherence $\boldsymbol{b}$-$\boldsymbol{c}$ [Fig. 7(a)], suggesting a possible path for the otherwise unexpected 30 cm^{-1} oscillation frequency observed for that peak. However, of the six 1CT paths leading to peak **10**—which shows oscillation only at 30 cm^{-1}—*two* paths go through the coherence $\boldsymbol{c}$-$\boldsymbol{a}$, which would add some amplitude to that peak which oscillates at 60 cm^{-1} during t_2. Also, of the seven paths leading to peak **1**, five would result in oscillation. Although peak **1** (and the other diagonal peaks and their overtones) does appear to oscillate weakly, the effect is not as prominent as in the cross peaks. This is posited to be a result of the combined contributions of the CT paths and the canonical (0CT) paths. Peak **1** is considerably stronger overall than peak **10**, for example, presumably because of the relative orientational responses in the 0CT paths and because of the added amplitude from the 1CT and 2CT paths. The only 0CT contribution to **1**, Y_{zzzz}^{aaaa}, is larger than the two combined 0CT (both of which correspond to Y_{zzzz}^{abab}) contributions to **10**. Thus, the oscillations in **1** sit atop a much larger background, and may be more difficult to observe as a result.

Considering the contributions to peaks **1**, **3**, and **10** from the t_1, t_3 2CT paths yields an even more surprising result. Of the 88 2CT paths which begin with excitation of mode $\boldsymbol{c}$, 48 contribute to the final trace over the density matrix and therefore to the total 2DIR signal. Of these, 13 contribute signal amplitude to peak **3**. More strikingly, *seven* of these are 30 cm^{-1} coherences during t_2. By contrast, only two of the ten 2CT paths leading to **12** include a coherence which would involve a 60 cm^{-1} oscillation. Thus we see that, although the 1CT paths are expected to contribute more amplitude to each peak per path than the 2CT paths (as the 1CT paths are statistically more likely), the net result in DMDC is actually determined heavily by the paths involving coherence transfers in both t_1 and t_3. Although we have confined our discussion here primarily to peaks **1**, **3**, and **10**, similar rules govern the other peaks: peak **16** has a parallel set of paths to those contributing to **3**, while peaks **2**, **7**, and **17** are analogous to peak **10**. It is possible that, given the relative dipole angles, certain coherence transfer processes are more likely than others. Ultimately, similar experiments and simulations will enable us to determine any guiding principles behind the relative likelihood of various types of coherence transfer.

V. CONCLUSION

We have presented a series of 2DIR spectra that resolve the coherent oscillations of various cross peaks as a function of the waiting time t_2. Because of the high frequency resolution available in multidimensional spectroscopy, we are able to correlate oscillations with specific excitations and emissions. In addition to assisting in the assignment of some of the spectral features in the 2D correlation spectrum, the waiting-time behavior in the system sheds light on some of the most fundamental aspects of excited state coherences between different vibrational modes. We have shown that, although single coherence transfer becomes important when two vibrational modes have parallel dipoles (owing to the contribution of otherwise orientationally vanishing paths), double coherence transfer paths must be included to fully account for the experimental observations. Further, based on comparison of the waiting-time coherence linewidths with those of the fundamental transitions, we conclude that the relative frequency fluctuations among the excited vibrational levels of DMDC in cyclohexane appear to be essentially uncorrelated. Future studies on other systems will seek to explore similar avenues while changing experimental parameters such as the extent and nature of intermode coupling by

studying different metal carbonyl systems, as well as by altering system-bath interactions using different solvents.

Despite the large extent to which we are able to understand the vibrational structure and dynamics of such a large and highly coupled molecule, much of the richness of energy, population, and coherence transfer in DMDC remains hidden due to occasional ambiguities in the spectral assignment presented here. This complexity will be addressed by a full computational treatment of the molecule: inclusion of the Raman active (IR dark) modes is likely to be crucial to understanding the full extent of coherence and population transfer in DMDC. The models needed to explain the phenomena observed here should be applicable to any strongly coupled system; the problem of the inclusion of dark states—including identifying when a dark state of similar frequency may be influencing dynamics—is absolutely critical to a full understanding of the high efficiency of natural photosynthetic systems, as well as vibrational energy flow in proteins and peptides.

ACKNOWLEDGMENTS

The authors wish to thank E. Geva and N. Preketes for useful discussions regarding the general nature of coherent energy transfer. This work was funded in part by a grant from the Rackham Graduate School, by the Petroleum Research Fund of the American Chemical Society and by the National Science Foundation (No. CHE-0748501).

[1] D. M. Jonas, Annu. Rev. Phys. Chem. **54**, 425 (2003).
[2] M. H. Cho, Chem. Rev. (Washington, D.C.) **108**, 1331 (2008).
[3] M. Khalil, N. Demirdoven, and A. Tokmakoff, J. Phys. Chem. A **107**, 5258 (2003).
[4] C. Kolano, J. Helbing, M. Kozinski, W. Sander, and P. Hamm, Nature (London) **444**, 469 (2006).
[5] A. T. Krummel and M. T. Zanni, J. Phys. Chem. B **110**, 13991 (2006).
[6] F. Ding, E. C. Fulmer, and M. T. Zanni, J. Chem. Phys. **123**, 094502 (2005).
[7] S. Woutersen, Y. Mu, G. Stock, and P. Hamm, Chem. Phys. **266**, 137 (2001).
[8] Y. S. Kim and R. M. Hochstrasser, Proc. Natl. Acad. Sci. U.S.A. **102**, 11185 (2005).
[9] J. R. Zheng, K. Kwak, J. Asbury, X. Chen, I. R. Piletic, and M. D. Fayer, Science **309**, 1338 (2005).
[10] J. R. Zheng, K. W. Kwak, J. Xie, and M. D. Fayer, Science **313**, 1951 (2006).
[11] M. Khalil, N. Demirdoven, and A. Tokmakoff, J. Chem. Phys. **121**, 362 (2004).
[12] J. A. Cina and G. R. Fleming, J. Phys. Chem. A **108**, 11196 (2004).
[13] G. S. Engel, T. R. Calhoun, E. L. Read, T. K. Ahn, T. Mancal, Y. C. Cheng, R. E. Blankenship, and G. R. Fleming, Nature (London) **446**, 782 (2007).
[14] H. Lee, Y. C. Cheng, and G. R. Fleming, Science **316**, 1462 (2007).
[15] J. B. Asbury, T. Steinel, K. Kwak, S. A. Corcelli, C. P. Lawrence, J. L. Skinner, and M. D. Fayer, J. Chem. Phys. **121**, 12431 (2004).
[16] M. L. Cowan, B. D. Bruner, N. Huse, J. R. Dwyer, B. Chugh, E. T. J. Nibbering, T. Elsaesser, and R. J. D. Miller, Nature (London) **434**, 199 (2005).
[17] N. Huse, B. D. Bruner, M. L. Cowan, J. Dreyer, E. T. J. Nibbering, R. J. D. Miller, and T. Elsaesser, Phys. Rev. Lett. **95**, 147402 (2005).
[18] J. D. Eaves, J. J. Loparo, C. J. Fecko, S. T. Roberts, A. Tokmakoff, and P. L. Geissler, Proc. Natl. Acad. Sci. U.S.A. **102**, 13019 (2005).
[19] Y. C. Cheng, G. S. Engel, and G. R. Fleming, Chem. Phys. **341**, 285 (2007).
[20] Y. J. Yan, R. M. Whitnell, K. R. Wilson, and A. H. Zewail, Chem. Phys. Lett. **193**, 402 (1992).
[21] Q. Wang, R. W. Schoenlein, L. A. Peteanu, R. A. Mathies, and C. V. Shank, Science **266**, 422 (1994).
[22] T. Kobayashi, T. Saito, and H. Ohtani, Nature (London) **414**, 531 (2001).
[23] A. Kahan, O. Nahmias, N. Friedman, M. Sheves, and S. Ruhman, J. Am. Chem. Soc. **129**, 537 (2007).
[24] T. Elsaesser, N. Huse, J. Dreyer, J. R. Dwyer, K. Heyne, and E. T. J. Nibbering, Chem. Phys. **341**, 175 (2007).
[25] J. R. Dwyer, J. Dreyer, E. T. J. Nibbering, and T. Elsaesser, Chem. Phys. Lett. **432**, 146 (2006).
[26] K. Heyne, N. Huse, J. Dreyer, E. T. J. Nibbering, T. Elsaesser, and S. Mukamel, J. Chem. Phys. **121**, 902 (2004).
[27] K. Heyne, N. Huse, E. T. J. Nibbering, and T. Elsaesser, J. Phys.: Condens. Matter **15**, S129 (2003).
[28] K. Heyne, N. Huse, E. T. J. Nibbering, and T. Elsaesser, Chem. Phys. Lett. **369**, 591 (2003).
[29] D. Madsen, J. Stenger, J. Dreyer, E. T. J. Nibbering, P. Hamm, and T. Elsaesser, Chem. Phys. Lett. **341**, 56 (2001).
[30] O. Golonzka, M. Khalil, N. Demirdoven, and A. Tokmakoff, J. Chem. Phys. **115**, 10814 (2001).
[31] M. J. Nee, R. McCanne, K. J. Kubarych, and M. Joffre, Opt. Lett. **32**, 713 (2007).
[32] K. F. Freed and A. A. Villaeys, Chem. Phys. **39**, 51 (1979).
[33] M. Hayashi and Y. Fujimura, J. Opt. Soc. Am. B **7**, 1653 (1990).
[34] M. Hayashi and Y. Fujimura, Chem. Phys. **140**, 41 (1990).
[35] E. Gershgoren, E. Gordon, and S. Ruhman, J. Chem. Phys. **106**, 4806 (1997).
[36] D. S. Kilin, O. V. Prezhdo, and M. Schreiber, J. Phys. Chem. A **111**, 10212 (2007).
[37] S. Palese, L. Schilling, R. J. D. Miller, P. R. Staver, and W. T. Lotshaw, J. Phys. Chem. **98**, 6308 (1994).
[38] O. Golonzka, M. Khalil, N. Demirdoven, and A. Tokmakoff, Phys. Rev. Lett. **86**, 2154 (2001).
[39] See EPAPS Document No. E-JCPSA6-129-641833 for a movie of the full set of 2DIR data as a function of t_2, a full list of biexponential fit parameters for non-oscillatory peaks, Lorentzian peak fits for each peak's t_2-dependent amplitude in frequency space, representative Lorentzian fits, and greater detail (including Feynman diagrams) regarding the available Liouville paths including coherence transfer. For more information on EPAPS, see http://www.aip.org/pubservs/epaps.html.
[40] F. A. Cotton and R. M. Wing, Inorg. Chem. **4**, 1328 (1965).
[41] S. H. Shim, D. B. Strasfeld, Y. L. Ling, and M. T. Zanni, Proc. Natl. Acad. Sci. U.S.A. **104**, 14197 (2007).
[42] J. J. Loparo, S. T. Roberts, and A. Tokmakoff, J. Chem. Phys. **125**, 194522 (2006).
[43] K. Lazonder, M. S. Pshenichnikov, and D. A. Wiersma, Opt. Lett. **31**, 3354 (2006).
[44] J. B. Asbury, T. Steinel, C. Stromberg, S. A. Corcelli, C. P. Lawrence, J. L. Skinner, and M. D. Fayer, J. Phys. Chem. A **108**, 1107 (2004).
[45] P. Mukherjee, I. Kass, I. T. Arkin, and M. T. Zanni, J. Phys. Chem. B **110**, 24740 (2006).
[46] A. V. Pisliakov, T. Mancal, and G. R. Fleming, J. Chem. Phys. **124**, 234505 (2006).
[47] L. Onsager, Phys. Rev. **38**, 2265 (1931).
[48] T. Jansen, D. Cringus, and M. S. Pshenichnikov, personal communication (April 2008).
[49] A. Piryatinski, V. Chernyak, and S. Mukamel, Chem. Phys. **266**, 285 (2001).
[50] A. Tokmakoff, J. Chem. Phys. **105**, 1 (1996).
[51] M. Khalil and A. Tokmakoff, Chem. Phys. **266**, 213 (2001).